Current-driven orbital order-disorder transition in $LaMnO_3$

Parthasarathi Mondal* and Dipten Bhattacharya†
Nanostructured Materials Division, Central Glass and Ceramic Research Institute, Council of Scientific and Industrial Research, Kolkata 700 032, India

P. Mandal
Experimental Condensed Matter Physics, Saha Institute of Nuclear Physics, Kolkata 700 064, India
(Received 31 January 2011; published 5 August 2011)

We report a significant influence of electric current on the orbital order-disorder transition in $LaMnO_3$. The transition temperature T_{OO}, thermal hysteresis in the resistivity ρ versus temperature T plot around T_{OO}, and latent heat L associated with the transition decrease with an increase in current density. Eventually, at a critical current density, L reaches zero. The transition zone, on the other hand, broadens with an increase in current density. The states at ordered, disordered, and transition zones are all found to be stable within the time window from $\sim 10^{-3}$ to $\sim 10^{4}$ s.

DOI: 10.1103/PhysRevB.84.075111 PACS number(s): 71.70.Ej, 64.60.Cn, 71.27.+a, 71.30.+h

I. INTRODUCTION

The long-range orbital order develops in $LaMnO_3$ with the ordering of active Mn $3d_{3x^2-r^2}$ and $3d_{3y^2-r^2}$ orbitals, alternately at each Mn site, within a Mn-O plane and the stacking of this order along the c axis (d-type order).[1] It undergoes a reversible order-disorder transition at a characteristic transition temperature T_{OO}.[2] The orbital order superstructure originates from cooperative fluctuations of the doubly degenerate Mn $3de_g^1$ orbitals interacting via a Kugel-Khomskii superexchange. This is further aided by the cooperative Jahn-Teller distortion of the $Mn^{3+}O_6$ octahedra.[3–5] The structurally forbidden orbital Bragg peaks could be clearly observed, with the expected azimuthal angle dependence of peak intensity, in resonant x-ray-scattering experiments, thus offering decisive evidence for the formation of an orbital order superstructure in $LaMnO_3$.[2] The orbital order, of course, is not a continuum but contains domains due to the interaction with intrinsic lattice strain and/or defects.[6] This orbital domain structure could also be observed in spatially resolved coherent x-ray-scattering experiments.[7] It is both technologically and fundamentally important to explore whether or not such an orbital ordered structure undergoes an order-disorder transition upon electric, magnetic, or optical stimulations. It has been shown that the long-range charge order in doped systems melts down under electric, magnetic, and optical stimulations, yielding a sharp rise in magnetization and/or conductivity together with a change in the crystallographic structures.[8–14] The orbital stripes too were shown to undergo rotation under an electric field in charge and/or orbital ordered layered manganites.[15,16] While in $LaMnO_3$, the Jahn-Teller distortion and orbital order was found to quench completely under a mechanical pressure of $\sim$20 GPa;[17] in $LaVO_3$, the high-energy laser pulse could melt the orbital order.[18] In spite of such a rich background, there is, as yet, no information about whether or not in undoped $LaMnO_3$ the orbital order-disorder transition can be driven by an electric field or photoirradiation. More importantly, in none of the past experiments on external-stimulation-driven phase transitions has an attempt been made to track the evolution of the order of the transition, i.e., how the latent heat of the transition, if any, varies with an increase in electrical, magnetic, optical, and mechanical energy, directly by calorimetry.

In this paper we report the observation of the significant influence of an electric current on the orbital order-disorder transition in $LaMnO_3$. Using the experimental data, a phase diagram on the current density-temperature J-T plane is constructed. We find that the latent heat L associated with the transition becomes zero at a critical current density $J_C \sim 50$ A/cm^2. It is also observed that the transition width broadens continuously as J is increased. The zones in the J-T plane—well below the transition, within the transition region, and well above the transition—are characterized by probing their resistivity relaxation behaviors together with the resistivity ρ versus temperature T patterns.

II. EXPERIMENTS

The experiments are carried out on a high-quality single crystal of $LaMnO_3$ of dimensions $5 \times 3 \times 1.5$ mm^3.[19] We also repeat the measurements on crystals of different thickness varying from 0.5 to 1.5 mm. The gold electrodes and wires are used in a standard linear four-probe configuration for the measurements of ρ-T and ρ versus time (at a given temperature) patterns under different bias currents. During the measurement of resistivity, the temperature sensor is attached directly onto the surface of the sample in order to record the data as a function of the actual sample temperature. We also record the differential thermal analysis (DTA) data simultaneously with the ρ-T measurements under varying bias current in order to estimate the latent heat of the transition, from the DTA peak around the transition point, as a function of applied current density. We report all the data as a function of the applied current density as the measurements are done by passing different bias current directly through the sample.

III. RESULTS AND DISCUSSION

In Fig. 1(a) we show the ρ-T data measured under different bias current. It is quite evident from the inset of Fig. 1(a) that the transition temperature T_{OO} decreases with

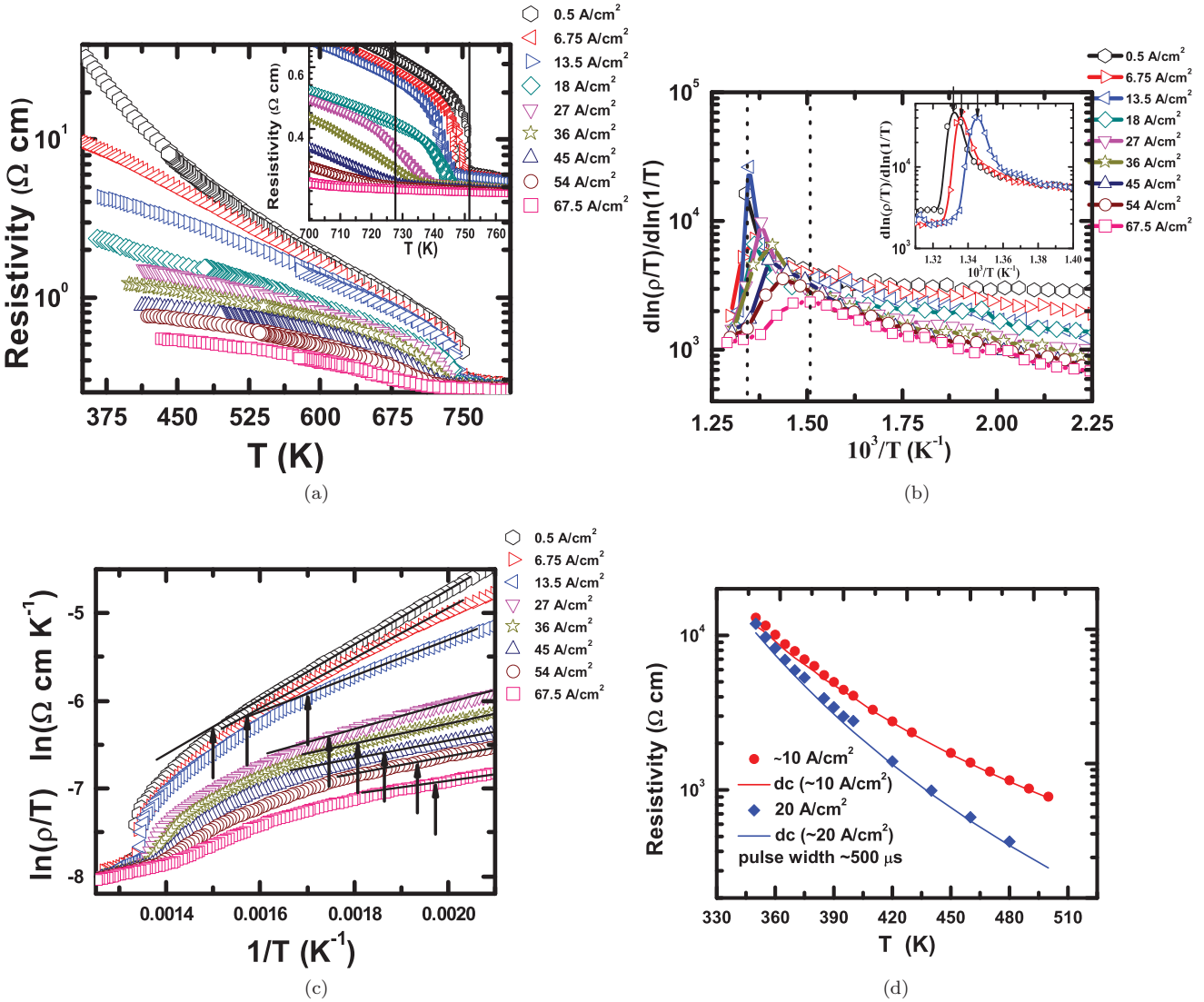

FIG. 1. (Color online) (a) Resistivity ρ versus temperature T plot for different bias currents, above room temperature, showing the variation in T_{OO} with the bias current density. The inset shows a closeup of the region around T_{OO}. (b) The $d\ln(\rho/T)/d(1/T)$ versus $1/T$ plots for different bias current densities obtained from the resistivity ρ versus temperature T data; the temperature corresponding to the peak is T_{OO}. The inset shows how T_{OO} shifts with an increase in current density in the low-current-density regime. (c) The $\ln(\rho/T)$ versus $1/T$ plots; the onset of the transition T^* is marked by an arrow. (d) Comparison of the data obtained from continuous dc and pulsed current measurements shown for two representative cases. In all the plots the current density increases as one moves from top to bottom.

increasing current (or bias voltage). In Fig. 1(b) we plot the $d\ln(R/T)/d(1/T)$ versus $1/T$ patterns. The peak in this plot marks T_{OO}; the height of the peak decreases while the width increases and the bias current increases. Figure 1(c) shows the deviation of the R-T pattern from the adiabatic small polaron hopping model $R = R_0T^{\alpha}\exp(\Delta/k_BT)$ ($\alpha = 1$) beyond a certain temperature T^* (marked in the figure by arrow) below T_{OO}. Therefore, T^* marks the onset of the transition. An error of $\pm 0.5\%$ is, of course, estimated to be involved in identifying T^*. Like T_{OO}, T^* also decreases progressively with the increase in bias current density. The zone confined within T^* and T_{OO} marks the transition zone where both orbital ordered and disordered phases are expected to coexist and the transport of charge carriers does not follow any model applicable to motion with long-range coherence.

An important issue here is the Joule heating of the samples, which renders the determination of the current-driven intrinsic effects difficult. In order to quantify the impact of Joule heating under an enhanced bias current (or electric field), we measure the increase in temperature due to heating by attaching a temperature sensor directly on the sample surface. Such an arrangement has been used by others to measure the actual sample temperature governed by both heating from the bath and Joule heating.[20] We found, as expected, that the increase in temperature as a result of current flow through the sample and sample-current lead junctions increases with the increase of current density J (from nearly negligible to as high as 100 K for a current in the range from 50 μA to 1 A). We start the current flow through the sample at room temperature and allow the temperature to increase by a certain extent within

that range. Once the temperature stabilizes at a particular point above room temperature we start the measurement. At that point no difference between the furnace (i.e., bath) and actual sample temperature could be noticed. The difference reduces to zero as the sample resistance and therefore the Joule heating drops drastically. The actual sample temperature has all along been monitored while recording the ρ-T data. Similar dc-driven measurements on charge ordered compound have been carried out by others and it was found that the impact of Joule heating is minimal.[14] In order to quantify the influence of Joule heating even further, we compare the dc resistivity pattern around T_{OO} with the pattern obtained under a pulsed current (with a pulse width of $\sim$500 μs). Both of the data sets are found to be nearly identical in the high-temperature regime [Fig. 1(d)], which establishes the negligible role of Joule heating in that zone. Moreover, the reproducibility of the features of the transition such as broadening of the peak in the DTA pattern, a decrease in the hysteresis and a jump in ρ-T around the transition, close matching of data between heating and cooling cycles in crystals of different thickness reveals that these are intrinsic field-driven effects. The experiments have been repeated on crystals of different thickness and all the features of the transition were found to be reproducible. The Joule heating cannot give rise to these features, namely, reproducibly, around T_{OO}.

Figure 2 shows the representative raw DTA thermograms recorded for different bias currents. With the increase in current, the peak broadens while the area under the peak decreases. Since the Joule heating near the transition zone is negligible, with an increase in J, the base line of the DTA trace does not change at all.[21] Therefore, no compensation is necessary to detect the peak and its variation for an increased current density. The latent heat is calculated by subtracting the background using an appropriate technique and properly identifying the peak area. The errors in such an estimation are calculated to be $\pm$0.5% in the case of transition temperatures and $\pm$10% in the case of latent heat. In Fig. 3(a) we show the variation in the latent heat L of transition with J while in Fig. 3(b) the variation of the transition temperatures is shown. There is a slight history effect as the transition temperatures and peak area differ a bit between heating and cooling cycles. This is not because of any intrinsic effect (e.g., due to slower phase transition dynamics or metastability) as discussed later, but could be due to a slight impurity in the inert atmosphere (flowing nitrogen) maintained during the experiment. In fact, the application of different heating and/or cooling rates did not result in any significant shift in the transition temperatures. The L is found to decrease gradually with an increase in J and reach zero at J_C $\sim$50 A/cm^2 [Fig. 3(a)]. This pattern of variation of L with J is consistent with the variation of the extent of

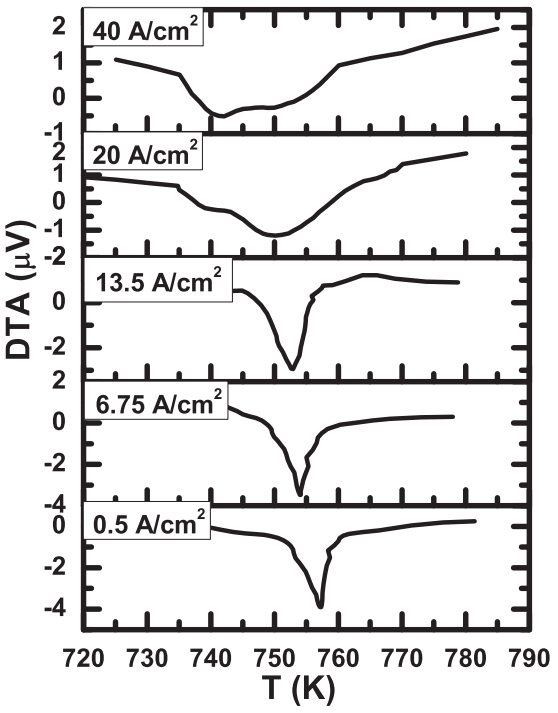

FIG. 2. Representative raw DTA traces in the heating cycle, observed for different bias currents, showing endothermic peaks around the orbital order-disorder transition; the peak shifts and broadens while the area decreases as the bias current increases.

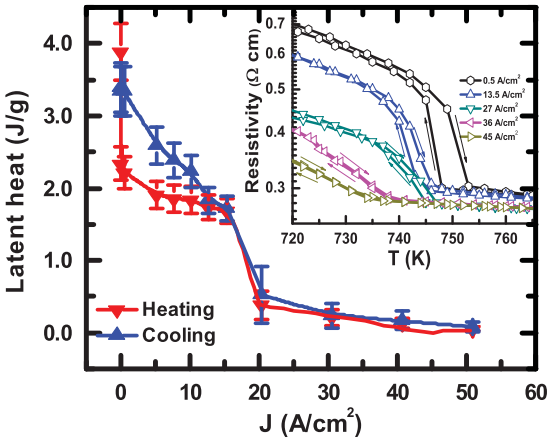

(a)

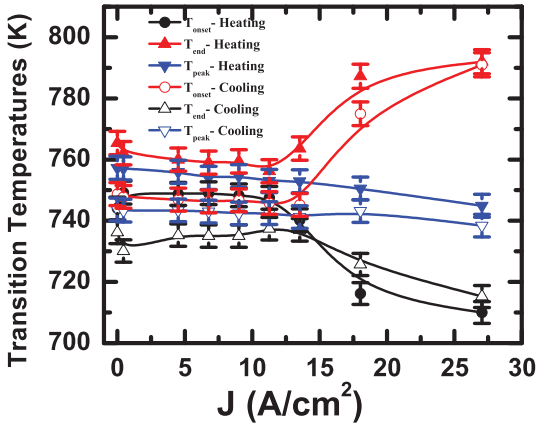

(b)

FIG. 3. (Color online) (a) Variation of the latent heat, estimated from the area under the peak observed in the DTA thermogram near the orbital order-disorder transition point, with bias current density J. The inset shows how the extent of hysteresis decreases with an increase in the bias current density; the current density increases from top to bottom in the inset; (b) Variation of the transition temperatures (noted from DTA thermograms) with J; obviously the transition width increases with J.

hysteresis ΔT in the ρ-T plot around T_{OO} between the heating and cooling runs; ΔT also decreases with an increase in J and vanishes at J_C [Fig. 3(a), inset]. The transition zone (marked by the onset, peak, and end temperatures) observed in Fig. 3(b) also broadens with J. It is important to mention here that the orbital order-disorder transition even in a very-high-quality single crystal of $LaMnO_3$ for nearly zero J is actually a broadened first-order transition.[22] No thermodynamic evidence for strictly first-order transitions has so far been reported. In comparison, compelling thermodynamic evidence for the first-order transition has been gathered using a local magnetization measurement in the case of vortex lattice melting in high-T_C superconductors. A steplike increase in magnetization could be noticed around a temperature of ~3 mK around the vortex lattice melting line.[23] It has also been shown that disorder can broaden the first-order transition.[24] In the present case, of course, the broadening of the transition even for a very low current density could be because of an intrinsic inhomogeneity or disorder due to the presence of orbital domains. Therefore, we compare the latent heat as a function of J only in the sense of noting the relative variation. The nature of the transition actually broadens progressively and finally becomes broader than the resolution of the instrument. At that point, the isolation of the peak area from the base line is no longer possible and the estimated L reaches zero. Using a calorimeter of higher sensitivity or a local calorimeter, one could possibly resolve the peak.

Using the data of transition temperatures as a function of bias current, obtained from both electrical and calorimetric measurements, we construct a phase diagram on the J-T plane (Fig. 4). The phase diagram indicates three regions: (i) ordered, (ii) disordered, and (iii) transition. It is clear from the figure that the transition zone broadens progressively with current density. Interestingly, the peak broadening, observed in DTA data for an increased J, covers a rather narrow portion of the T^*-T_{OO} transition zone identified from the electrical resistivity

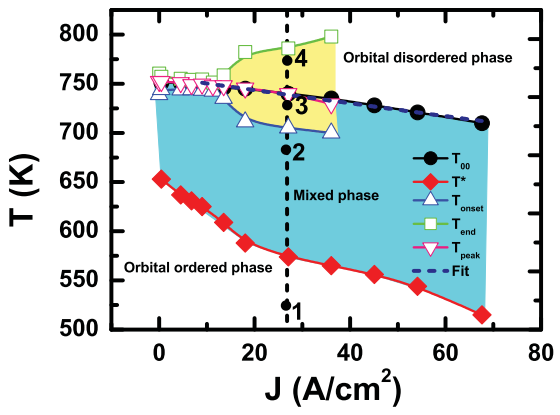

FIG. 4. (Color online) Phase diagram of the electric-current-driven orbital order-disorder transition on the J-T plane; the transition width increases with an increase in J. The peak width of the DTA data has been superimposed on the phase diagram. It shows that the DTA peak width is quite small in comparison to the transition width identified from the electrical resistivity data. For clarity, the error bars have been omitted here. The points at which the data of relaxation of resistivity are presented in Fig. 5 are shown as 1, 2, 3, and 4.

data. It shows that although the electrical measurement senses the onset of the transition at T^*, the calorimetric measurement senses the onset at a much higher temperature closer to the thermodynamic T_{OO}. Earlier work[25] on the evolution of the crystallographic structure across T^*-T_{OO}, on the contrary, reveals that the anomalous structural distortion sets in at $\sim T^*$ itself. The reason behind the discrepancy between the onset points identified from the crystallographic and resistivity data and those recorded from the calorimetric data could be the difference in the sensitivity of the probes. The calorimeter sensitivity is $\leqslant 1$ μW whereas the sensitivity of the nanovoltmeter used to record the voltage drop and hence resistance of the sample is $\leqslant 10$ nV. Therefore, while the electrical resistivity and x-ray-diffraction experiments could sense the nucleation of the orbital disordered phase and hence record accurately the onset of transition, the calorimeter could record the onset of the transition only when the orbital disordered phase has grown beyond a critical size and hence at a higher temperature.

In order to probe further the characteristics of these three regions of the J-T phase diagram, in particular whether or not the slight history effect observed in DTA data around the transition is due to an intrinsic metastability of the phases at the transition zone, we measure the relaxation of the resistivity. To cross the boundaries of the transition zone along a constant J line we select four points (shown in Fig. 4) with different temperatures. The relaxation measurements are carried out by increasing the temperature of the crystal to the desired point and then applying the requisite current density. We reach the points separately by increasing the temperature and field from room temperature and zero field. The resistivity data are recorded over a time span from ~50 ms to 3600 s at an interval of ~50 ms after stabilizing the sample temperature at a given point within less than 0.01 K. We repeat such measurements along other constant J lines too. In Fig. 5 we show the relaxation characteristics observed at points 1, 2, 3, and 4. The characteristics are representative of all the points at which similar relaxation measurements are carried out. We observe virtually no time dependence of the resistivity corresponding to the points 1, 2, 3, and 4, which signifies the stability of not only orbital ordered and disordered phases but also of the mixed phase within the transition zone. Therefore, the states at the transition zone are not metastable. The slight difference observed in the transition temperatures between heating and cooling cycles (Fig. 3) cannot be due to metastability and the consequent emergence of transient states around the transition. The transition is thermodynamic and the transition kinetics is not accessible within the laboratory time window $\sim 10^{-3} - 10^4$ s at all the temperatures. Probing the evolution of the crystallographic structure[25] within and around the transition zone shows that the O' orthorhombic structure ($c/\sqrt{2} < a < b$; a, b, and c are lattice parameters) of the orbital ordered phase evolves into a mixed O' and O orthorhombic phase within the transition zone and finally into a pure O orthorhombic phase ($c/\sqrt{2} \sim a \sim b$) above the transition zone. By taking into consideration the evolution of the structure within the transition zone along with the relaxation data of resistivity, it is possible to conclude that the mixed $O' + O$ phase does not have any temporal fluctuation within the laboratory time window. In contrast, the orbital ordered phase in nanoscale (<20 nm) $LaMnO_3$ is found to be

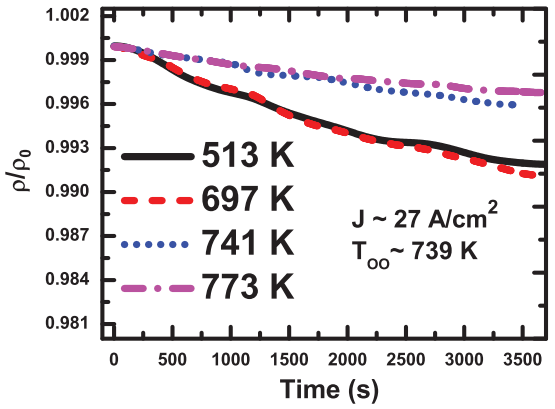

FIG. 5. (Color online) Representative plot of the time dependence of the normalized electrical resistance at different temperatures for a bias current density of $\sim$27 A/cm^2. The temperatures and the bias current are chosen in such a way that that different regions of the phase diagram—ordered, disordered, and transition—can be accessed. The extent of relaxation appears to be negligible in all the cases, indicating stability of the phases. In contrast, a 2%-4% decay in resistance could be noticed[26] in the case of the metastable orbital ordered phase in nanoscale ($\leqslant$ 20 nm) $LaMnO_3$.

metastable with a 2%–4% decay in the resistance with time and an irreversible order-disorder transition within a similar time scale.[26] The emergence of transient metastable states with a lifetime ($\sim 10^{-3}-10^{4}$ s) comparable to the laboratory time scale has been observed by Kalisky *et al.*[27] around the vortex solid-solid phase transition as well, in a high-T_C superconductor.

The decrease in T_{OO} as well as latent heat and hysteresis associated with the transition possibly result from the electric-current-driven depinning of orbital domains. The orbital ordered phase even in stoichiometric $LaMnO_3$ is not a continuum under zero electric current. It contains domains due to the interaction with intrinsic electronic and/or lattice defects, strain, etc.[6,7] Like in the case of charge density waves in solids,[28] these intrinsic defects act as pinning centers for orbital domains as well. In fact, the orbital order-disorder transition takes place via depinning of orbital domains.[29] In the orbital disordered state, the short-range order, with high mobility and hence temporal fluctuations, prevails.[30] The application of an increased current density (bias field) leads to the electromigration of defects,[31] which in turn can give rise to the field-driven depinning transition. The depinning transition of charge density waves as well as the vortex lattice in high-T_C superconductors has been thoroughly studied.[32] It has been shown that, depending on the concentration of pinning centers and applied force, the depinning of the charge density waves can follow either a two-stage or a single-stage process. If the concentration of defects is strong, the domains start sliding plastically under a small force, which finally gives way to a sharp transition into a coherent collective movement in three dimensions under higher force. In contrast, in the case of weak disorder or a low concentration of defects, the depinning transition becomes a continuous process and continuously yields a coherently moving collective state. The weak disorder model predicts that the depinning transition yields an exponential variation of the transition energy scale (e.g., transition temperature) with the applied force.[33] Interestingly, this model is found to be valid in the present case. It has been observed that the T_{OO} versus current density J pattern (Fig. 4) follows closely the model $T_{OO}(J)/T_{OO}(0) = \exp(-J/J_0)$ (Fig. 4, dashed line), except at a very low J (J_0 is a constant here and T_{OO} is the transition temperature under zero field). The validity of this model in the present case provides indirect support for the conjecture of current-density- (bias field) driven depinning of orbital domains. Because of the variation in the depth of the potential well of the defects, the screening of the direct force for electromigration will vary,[34] which in turn is expected to give rise to inhomogeneous depinning. This inhomogeneous depinning is possibly the origin of the broadening of the orbital order-disorder transition zone and drop in latent heat.

The question remains whether there can be any other origin for the influence of the electric field on the orbital order in $LaMnO_3$? The d-type orbital order in $LaMnO_3$ cannot give rise to an electric dipole moment. It produces only a higher-order quadrupole moment,[35] which cannot couple linearly with the applied electric field. Even the domain boundaries of the orbital order cannot be intrinsically charged. Therefore, unlike charge order, microscopically, long-range orbital order in $LaMnO_3$ should not be influenced by the electric field. It may be asked whether unleashing the charge carriers via $Mn^{3+} \rightarrow Mn^{2+} + Mn^{4+}$ disproportionation under field conditions could then be the origin of such an effect? The generation of mobile charge carriers under field conditions would have given rise to an even more dramatic effect. Therefore, it seems that these effects are not really playing any significant role here. The study of the orbital domain structure for an external electric field using spatiotemporally resolved resonant x-ray-scattering data can offer direct proof of the orbital domain depinning transition under field conditions. This is beyond the scope of this paper.

IV. CONCLUSION

In summary, we observed a significant influence of electric current density (bias field) on the orbital order-disorder transition in a single crystal of pure $LaMnO_3$. The transition temperature, hysteresis, and latent heat of the transition decreased monotonically with an increase in the current density; the transition width, in contrast, increased. Finally, at a critical current density, the latent heat became zero. The states at the ordered, disordered, and transition zones were all found to be thermodynamically stable within the laboratory time scale. This current-density-driven orbital order-disorder transition possibly originated from the field-driven depinning of orbital domains via electromigration of intrinsic defects.

ACKNOWLEDGMENTS

We acknowledge helpful discussions with R. Nath, A. K. Raychaudhuri, T. Saha-Dasgupta, and D. I. Khomskii. P. M. acknowledges financial support from Council of Scientific and Industrial Research during this work.

*Present address: Department of Advanced Material Science and Engineering, Sungkyunkwan University, Suwan 440-706, Korea.
†Corresponding author: dipten@cgcri.res.in

[1]T. Mizokawa, D. I. Khomskii, and G. A. Sawatzky, Phys. Rev. B **60**, 7309 (1999).
[2]Y. Murakami, J. P. Hill, D. Gibbs, M. Blume, I. Koyama, M. Tanaka, H. Kawata, T. Arima, Y. Tokura, K. Hirota, and Y. Endoh, Phys. Rev. Lett. **81**, 582 (1998).
[3]K. I. Kugel and D. I. Khomskii, Zh. Eksp. Teor. Fiz. **64**, 1429 (1973) [Sov. Phys. JETP **37**, 725 (1973)]; Sov. Phys. Usp. **25**, 231 (1982).
[4]S. Okamoto, S. Ishihara, and S. Maekawa, Phys. Rev. B **65**, 144403 (2002).
[5]E. Pavarini and E. Koch, Phys. Rev. Lett. **104**, 086402 (2010).
[6]K. H. Ahn and A. J. Millis, Phys. Rev. B **64**, 115103 (2001).
[7]See, for example, C. S. Nelson, J. P. Hill, D. Gibbs, F. Yakhou, F. Livet, Y. Tomioka, T. Kimura, and Y. Tokura, Phys. Rev. B **66**, 134412 (2002).
[8]Y. Tomioka, A. Asamitsu, Y. Moritomo, H. Kuwahara, and Y. Tokura, Phys. Rev. Lett. **74**, 5108 (1995).
[9]A. Asamitsu, Y. Tomioka, H. Kuwahara, and Y. Tokura, Nature (London) **388**, 50 (1997).
[10]K. Miyano, T. Tanaka, Y. Tomioka, and Y. Tokura, Phys. Rev. Lett. **78**, 4257 (1997).
[11]V. Kiryukhin, D. Casa, J. P. Hill, B. Keimer, A. Vigliante, Y. Tomioka, and Y. Tokura, Nature (London) **386**, 813 (1997).
[12]S. Yamanouchi, Y. Taguchi, and Y. Tokura, Phys. Rev. Lett. **83**, 5555 (1999).
[13]M. Hervieu, A. Barnabé, C. Martin, A. Maignan, and B. Raveau, Phys. Rev. B **60**, R726 (1999).
[14]C. N. R. Rao, A. R. Raju, V. Ponnambalam, S. Parashar, and N. Kumar, Phys. Rev. B **61**, 594 (2000).
[15]K. Hatsuda, T. Kimura, and Y. Tokura, Appl. Phys. Lett. **83**, 3329 (2003).
[16]D. Polli, M. Rini, S. Wall, R. W. Schoenlein, Y. Tomioka, Y. Tokura, G. Cerullo, and A. Cavalleri, Nature Mater. **6**, 643 (2007).
[17]I. Loa, P. Adler, A. Grzechnik, K. Syassen, U. Schwarz, M. Hanfland, G. Kh. Rozenberg, P. Gorodetsky, and M. P. Pasternak, Phys. Rev. Lett. **87**, 125501 (2001).
[18]S. Tomimoto, S. Miyasaka, T. Ogasawara, H. Okamoto, and Y. Tokura, Phys. Rev. B **68**, 035106 (2003).
[19]P. Mandal, B. Bandyopadhyay, and B. Ghosh, Phys. Rev. B **64**, 180405(R) (2001).
[20]A. S. Carneiro, R. F. Jardim, and F. C. Fonseca, Phys. Rev. B **73**, 012410 (2006).
[21]The sensitivity of the DTA sensor is $\sim$1 μW.
[22]J.-S. Zhou and J. B. Goodenough, Phys. Rev. B **68**, 144406 (2003).
[23]E. Zeldov, D. Majer, M. Konczykowski, V. B. Geshkenbein, V. M. Vinokur, and H. Shtrikman, Nature (London) **375**, 373 (1995).
[24]A. Soibel, E. Zeldov, M. Rappaport, Y. Myasoedov, T. Tamegai, S. Ooi, M. Konczykowski, and V. B. Geshkenbein, Nature (London) **406**, 282 (2000); W. K. Kwok, S. Fleshler, U. Welp, V. M. Vinokur, J. Downey, G. W. Crabtree, and M. M. Miller, Phys. Rev. Lett. **69**, 3370 (1992); Y. Imry and M. Wortis, Phys. Rev. B **19**, 3580 (1979).
[25]See, for example, G. Maris, V. Volotchaev, and T. T. M. Palstra, New J. Phys. **6**, 153 (2004).
[26]P. Mondal, D. Bhattacharya, A. Maity, O. P. Chakrabarti, A. K. M. Maidul Islam, and M. Mukherjee, J. Appl. Phys. **109**, 084327 (2011).
[27]B. Kalisky, Y. Bruckental, A. Shaulov, and Y. Yeshurun, Phys. Rev. B **68**, 224515 (2003).
[28]G. Gruner, *Density Waves in Solids* (Addison-Wesley, Reading, MA, 1994).
[29]See, for example, M. Uchida, R. Mathieu, J. He, A. Asamitsu, R. Kumai, Y. Tomioka, Y. Matsui, and Y. Tokura, J. Phys. Soc. Jpn. **75**, 053602 (2006).
[30]X. Qiu, Th. Proffen, J. F. Mitchell, and S. J. L. Billinge, Phys. Rev. Lett. **94**, 177203 (2005).
[31]R. S. Sorbello, in *Solid State Physics*, edited by H. Ehrenreich and F. Spaepen (Academic, San Diego, 1997), Vol. 51, p. 159.
[32]V. M. Vinokur and T. Nattermann, Phys. Rev. Lett. **79**, 3471 (1997).
[33]P. Monceau, in *Charge Density Waves in Solids*, edited by G. Y. Hutiary and J. Solyom (Springer, Berlin, 1985).
[34]A. Lodder, Europhys. Lett. **72**, 774 (2005).
[35]A. Sartbaeva, S. A. Wells, M. F. Thorpe, E. S. Bozin, and S. J. L. Billinge, Phys. Rev. Lett. **99**, 155503 (2007).